Schumacher, P. N., E. Centeno, B. Wu, and K. Gallo, 2026: Evaluation of *GOES* satellite data for use in the Grassland Fire Danger Index. *J. Operational Meteor.*, **14** (9), 129−144, doi: https://doi.org/10.15191/nwajom.2026.1409.

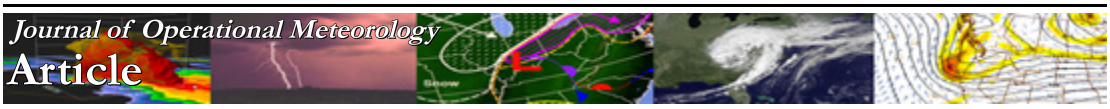

Evaluation of GOES Satellite Data for use in the Grassland Fire Danger Index

PHILIP N. SCHUMACHER
Cooperative Institute for Research in the Atmosphere, Colorado State University, Affiliate working on a cooperative agreement/grant with NOAA/Global Systems Laboratory, Boulder, Colorado

EMMA CENTENO
American Forests, San Francisco, CA

BRITNEY WU
Jacobs Engineering Group, Inc, San Francisco, CA

KEVIN GALLO
Brevard, NC

(Manuscript received 16 April 2025; review completed 3 November 2025)

ABSTRACT

Determining fire fuel status remains a challenge across the Great Plains of the United States, where grasses and shrubs are the primary land covers and fuels for fires. This study compared two methods of estimating the Curing Index, an indicator of the moisture level of vegetation, that is included in the Grassland Fire Danger Index (GFDI): i) a satellite method using data acquired by the *Geostationary Operational Environmental Satellite (GOES)* Advanced Baseline Imager and ii) a method using a Growing Season Index (GSI) that includes observed meteorological conditions to estimate plant growth.

Curing Index (CI) values were calculated for 2021 and 2022 at 47 Remote Automated Weather Stations (RAWS) that had dominant land cover types of either grassland or shrubland vegetation. Differences in the Curing Index of >50% were observed at various times from spring through autumn between the two methods. Differences in Curing Index between the two methods resulted in differences in GFDI, which changed the fire danger rating category within the National Fire Danger Rating System. The greatest differences in grassland and shrubland GFDI values included greater values of GFDI in the summer months when GSI was used to compute the CI. Also, during both years, the CI computed with the GSI displayed an autumn green-up during a dry early autumn that was not observed by satellite data. The early autumn green-up displayed by the GSI-based CI, when vegetation is normally in senescence, was attributed to a decrease in the vapor pressure deficit component of the GSI.

1. Introduction

Wildfires can have significant and lasting effects on both the natural and built environment. Wildfires are both a critical part of a healthy ecosystem by removing diseased or dead vegetation and allowing seeds to germinate. They can also be responsible for devastating swaths of damage and often result in considerable losses in grassland and rangeland as well as homes and infrastructure. Estimates by the National Oceanic and Atmospheric Administration (NOAA) of the total cost to property damage due to wildfires between 2015 and 2024 (NOAA 2024) within the United States ranged from $22.9 million (2015) to $19.1 billion (2018) dollars. In addition to the property damage, the wildfire events resulted in 3 (2019) to 103 (2023) fatalities and 17 (2016) to 182 (2020) injuries.

Corresponding author address: Philip N. Schumacher, 5312 E. 28th St., Sioux Falls, SD 57110
E-mail: philip.schumacher@colostate.edu

Wildfires have become more common in the grasses, ranges, and shrublands of the United States Great Plains fueled by high temperatures, high winds, and low humidity (Lindley et al. 2011). Two recent examples occurred in Kansas and Nebraska. On 15 December 2021, several large grassland/rangeland (hereafter only grassland will be used unless referring to official National Weather Service [NWS] products) fires consumed >66 000 hectares (>163 000 acres, NOAA 2021a) in Kansas resulting in >$2.4 million of damage and two deaths. (NOAA 2021b). On 22–23 April 2022, several wildfires occurred across Nebraska, Kansas, and South Dakota. One fire in south central Nebraska consumed >17 000 hectares (>44 000 acres) resulting in one death (NOAA 2022a). Predicting conditions favorable for the rapid spread of grassland fires is a goal of the National Oceanic and Atmospheric Administration's (NOAA) National Weather Service (NWS) as well as other land management agencies. For several decades, NWS offices across the Great Plains have been issuing Rangeland Fire Danger statements to alert the public and emergency officials when conditions are favorable for dangerous grassland fires (e.g., www.weather.gov/fsd/fire). In the 2010s, NOAA's Grassland Fire Danger Index (GFDI) was adapted by several NWS offices in the central United States (Schreck et al. 2010) from a model presented in Nobel et al. (1980) widely used in Australia. The GFDI is used to estimate the level of fire danger in the Great Plains using hourly forecast meteorological data (temperature, sustained wind, and relative humidity) and estimates of the vegetation moisture content (Curing Index). The maximum hourly GFDI in a 24-h day is converted to a National Fire Danger Rating System (NFDRS) category to create a daily Fire Danger forecast that is shared with the public and fire weather partners through Rangeland Fire Danger statements issued by the NWS. One deficiency of the GFDI is that Curing Index (CI) only provides information on the greenness or brownness of vegetation. Additionally, CI does not provide information on the amount of dried fuels that exist for combustion nor does it measure if some of the dried fuels may be moist due to recent rainfall or dew. Therefore, it cannot differentiate between locations where abundant dry fuels results in extreme fire behavior and areas where low amounts of dried fuels may burn but are unlikely to grow rapidly.

More recently, additional methods and models have been used to determine the susceptibility of fuels to fire start and spread. As a preliminary component of this study, an internal survey was made of 25 NWS offices in the Great Plains related to their methods for determining fuel status. Of the 18 NWS offices responding, 56% indicated that for determining fuel status (i.e., vegetation moisture content), they used: i) vegetative models based upon meteorological data, ii) a combination of observations of fuels and a vegetative model, iii) the Energy Release Component (ERC) which also uses a meteorological-based model (Cohen and Deeming 1985, Lindley et al. 2014). One vegetation phenological model used or tested by NWS offices to estimate the CI is called the Growing Season Index (GSI, Jolly et al. 2005) that also relies on meteorological observations. One limitation of the field observation and meteorological model methods of estimating the CI is that they rely on interpolation of data from point observations to grid cells that span large areas, e.g., the Great Plains region.

The remainder of offices (44%) used satellite, visual observations of local vegetation or a combination to estimate the CI. Visual observations of 100% green vegetation are assumed to have a 0% CI, which according to Schreck et al. (2010) is "typically seen from late spring to mid-summer across the Central Plains." Observations of 0% green vegetation have a CI of 100% and "represents fully cured, dry grass typically seen from late fall into early spring across the Central Plains." (Schreck et al. 2010). Satellite-derived data can provide spatially cohesive and distributed observations of the land surface. The Normalized Difference Vegetation Index (NDVI, Eq. 1) and related products derived from the NOAA Advanced Very High Resolution Radiometer (AVHRR) data have been previously demonstrated and used to assess vegetation greenness and vegetation condition for use in fire danger assessments (e.g., Burgan and Hartford, 1993 and Burgan et al. 1996). Currently a Green Vegetation Fraction (GVF) product is available from the follow-on sensor to the AVHRR, the Visible Infrared Imaging Radiometer Suite (VIIRS). The GVF was specifically developed to provide an estimate of the percentage of green vegetation within a grid cell (JPSS, 2019). Like visual observations, the GVF is inversely related to the CI such that a GVF value of 100% (0%) indicates the presence of only (no) green vegetation. The GVF product is available for the conterminous United States at a 1 km spatial resolution and may provide supplemental or improved information related to the CI used in the GFDI. A limitation of the current VIIRS-based GVF product is that it is usually limited to one

daytime observation per day (per sensor) due to the orbital characteristics of the platform that carries the sensor. The current series of Geostationary Operational Environmental Satellite (*GOES*) satellites (*GOES-R* series) include the Advanced Baseline Imager (ABI) sensor (Schmit et al. 2017). The ABI sensor, unlike previous *GOES* satellites, includes a near-IR channel that can be used to routinely derive vegetation-related indices at an interval of every five min (12 observations per hr). The increased observation frequency available with the ABI can provide a significantly greater opportunity for cloud-free observations of the vegetated land surface. A satellite-derived GVF could provide a more spatially accurate estimate of the CI than the point-based and interpolated GSI product.

In this study, the use of a satellite-derived GVF product was i) estimated from *GOES* ABI data and ii) evaluated and compared with the Growing Season Index (GSI) for estimation of a vegetation Curing Index and its use within the GFDI. GSI was chosen for comparison because it is currently being tested by NWS offices as a means to estimate the CI. The focus of this study is the grass and shrubland regions within the United States Great Plains.

2. Data and methods

a. Estimation of GVF from Advanced Baseline Imager NDVI

The routinely produced GVF product, available on a daily basis as the mean of a moving 7-day interval (using only clear-sky observations) was developed using the NOAA VIIRS sensor data that nominally includes a single daytime observation. The regional 1-km spatial resolution VIIRS GVF product (NESDIS, 2021) was used as ground truth in this analysis as available from NOAA's Comprehensive Large Array-data Stewardship System (CLASS, NOAA 2023). The *GOES* ABI provides 12 observations per hr, thus affording a greater likelihood of clear-sky observations. The *GOES-16* ABI Channel 2 and 3 data acquired at 1500 UTC were downloaded in a 7-day interval to: i) match the nominal acquisition dates and times of the VIIRS data used to derive the GVF product, and ii) to coincide with a minimum in cloud cover during the warm season in the Great Plains that is caused by cumulus that form due to heating later in the day (Betts and Tawfik, 2016). Other clouds not tied to diurnal heating, such as cirrus associated with a jet streak, may still obscure the surface. The *GOES-16* ABI data were retrieved from Amazon Web Services (noaa-goes16.s3.amazonaws.com/index.html). NDVI is a way to measure greenness of vegetation from satellite using the formula:

$$\text{NDVI} = (\text{near-IR} + \text{visible}) / (\text{near-IR} - \text{visible}) \quad (1)$$

where visible is from ABI Channel 2 (0.60–0.68 μm) and near-IR is from ABI Channel 3 (0.85–0.88 μm). The maximum 7-day NDVI value Eq. (1) was derived for each pixel excluding values when the *GOES* cloud mask product indicated that clouds were present. If all 7 days were cloudy, NDVI was listed as missing for that pixel. The 7-day ABI-derived NDVI values were compared with the VIIRS-derived GVF values for the same temporal intervals. Both data were cloud-screened using the ABI daily Clear Sky mask (www.goes-r.gov/products/baseline-clear-sky-mask.html).

Linear regression models Eq. (2) between the GVF and ABI NDVI were developed at 51 Remote Automated Weather Stations (RAWS, raws.nifc.gov/sites/default/files/inline-files/NWCG%20Standards%20for%20Fire%20Weather%20Stations_2019_1.pdf, Fig. 1) for two wildfire susceptible land cover types, grasslands and shrublands, within the United States Great Plains based on the 2021 USDA Cropland Data Layer database (CDL: Boryan et al. 2011):

$$\text{GVF}_x = b_o + b_1 (\text{NDVI}) \quad (2)$$

where x indicates whether the model was developed for grassland (g) or shrubland (s). Cropland was excluded from this analysis as the NWS does not routinely use the CI from crops to forecast fire danger. The developed models for grassland and shrublands were further evaluated using an analysis of the sum of squares associated with the models to determine if individual models were required or a combined model was sufficient.

The models were based on GVF and ABI NDVI data obtained during 2021 for 3 × 3 km areas centered on the RAWS stations within the Great Plains that displayed a minimum of seven of the nine 1-km grid cells (>75% of their surrounding area) as either grassland or shrubland based on the CDL information that was aggregated from a 0.5 to 1 km resolution to match the satellite products. There were 28 grassland stations and 23 shrubland stations used in the analysis (Fig. 1). The distribution of RAWS stations defined as grassland and shrubland was impacted by the increased percentage of land used for

crops when moving west to east across the Great Plains resulting in most stations being located west of 100ºW. Also, shrubland is the predominant land cover primarily in areas south of 35ºN. As a result, most grassland locations used in this study were located north of 40ºN and most shrubland stations were south of 35ºN (Fig. 1). The models were based on GVF and ABI NDVI data obtained for the first week of each month, March through November of 2021, to assure inclusion of the growing season within the study region.

b. Development of Curing Index estimates

CI estimates, ranging from a value of 0% to 100%, were derived from both the GSI (based on RAWS meteorological observations) and the ABI-derived GVF (hereafter GVF), based on satellite-derived information at the RAWS stations that were included in the development of the GVF equation above. There were 25 grassland and 22 shrubland locations that met the land cover criteria described in section 2a and had meteorological data available for at least a portion of 2021 and 2022 (Fig. 1). For this analysis, the 7-day maximum NDVI was found for each 7-day period beginning with 1–7 March and ending 22–28 November for both 2021 and 2022. Although many severe fires occur from December–February in the Great Plains, the vegetation is dormant at this time and fire spread is primarily a function of meteorological conditions. From March–November, the CI is changing as vegetation grows and then becomes dormant. Therefore, fire growth and spread are a function of both changes in atmospheric conditions and live fuel moisture. The *GOES*-ABI data for estimating the CI were obtained from Amazon Web Services at 1500 UTC to minimize cloud cover across the study area. In order to calculate the 21-day mean GSI ending on 1 March, meteorological information needed to compute GSI were retrieved from the RAWS database maintained by Synoptic Data (synopticdata.com/) from 8 February through 1 December of 2021 and 2022. No additional quality assurance was done with the data. The daily GSI (iGSI, Jolly et al. 2005) is the product of scaled (0 to 1) daily indicators (i) of minimum temperature (iT_{min}), vapor pressure deficit (iVPD), and photoperiod (iPhoto):

$$iGSI = iT_{min} \times iVPD \times iPhoto \quad (3)$$

Table 1 shows the minimum and maximum values for the scaling of each of the GSI parameters. With the exception of VPD, any value at or below the minimum value is 0 and above the maximum value is 1. The formula for calculating the photoperiod (Photo) is from Brock (1981 as shown in Forsythe et al. (1995)), where iPhoto (Table 1) is the scaled length of day (D, Eq. 4):

$$D = 2\frac{hourAngle}{15} \quad (4)$$

where

$$hourAngle = \cos^{-1}(-\tan(L)\tan(\phi)) \quad (5)$$

$$\phi = 23.45 \sin 360\left(\frac{283 + J}{365}\right) \quad (6)$$

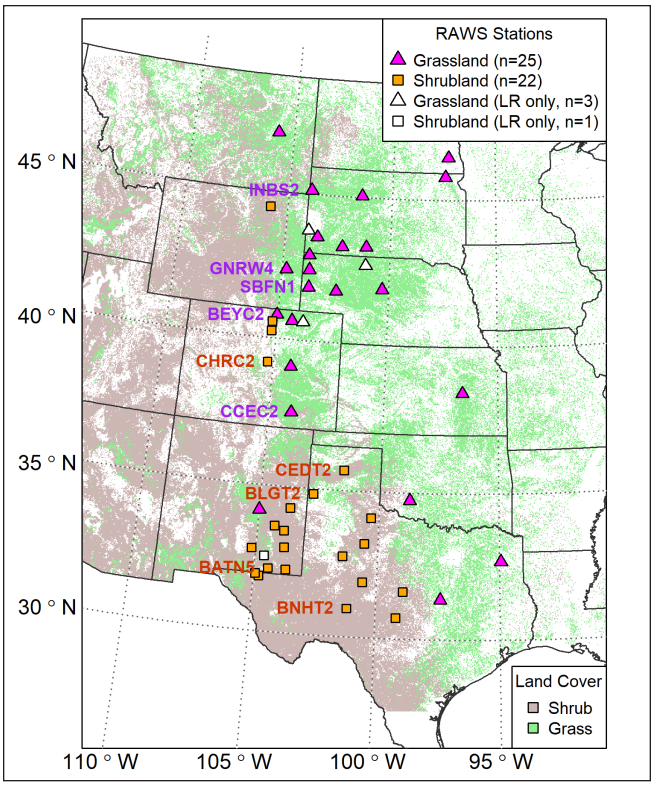

Figure 1. Locations of RAWS stations used for development of linear regression models relating NDVI to GVF and for evaluation of Curing Indices. Orange filled squares are the locations of stations primarily with shrub landcover and magenta filled triangles are the locations of stations with grass landcover. White squares (triangles) are locations only used for development of linear regression (LR) models. Landcover based upon the USDA CDL in 2021 are colored where grasses (light green) or shrubs (tan) predominate. Stations used in Fig. 8 have the station identifier listed to the left of their location. *Click image for an external version; this applies to all figures hereafter.*

Table 1. The minimum and maximum values for the variables used to scale components of GSI, as per Jolly et al. (2005).

Parameter	Minimum Value	Scaled Minimum	Maximum Value	Scaled Maximum
iT_{min}	–2ºC	0.0	5ºC	1.0
iVPD	900 Pa	1.0	4100 Pa	0.0
iPhoto	10 h	0.0	11 h	1.0

D is the length of day, ϕ is the sun's declination angle, L is the latitude, and J is the Julian day. To calculate VPD, the T_{max}, T_{min}, RH_{max}, and RH_{min} were retrieved for each day at the RAWS station. Allen et al. (1998) Eqs. (11) and (12) were used to find the saturated vapor pressure as follows:

$$e(\mathrm{T}) = 0.6108e^{\frac{1727T}{T+237.3}} \tag{7}$$

$$e_s = \frac{e(T_{max}) + e(T_{min})}{2} \tag{8}$$

where $e(T)$ is the vapor pressure at temperature T and e_s is the saturated vapor pressure. Then the average vapor pressure during the day from Allen et al. (1998) Eq. (17) is:

$$e_a = \frac{e\left(T_{max}\right)\frac{RH_{min}}{100} + e\left(T_{min}\right)\frac{RH_{max}}{100}}{2} \tag{9}$$

The VPD is then the difference between e_s and e_a, and iVPD (Table 1) is the scaled VPD.

Additionally, the daily GSI was the average of a 21-day moving window (Jolly et al. 2005). The GSI was used to estimate the Live Fuel Moisture (LFM). For GSI (NWCG, 2023) as per Eq. (3) (C. Schultz, personal communication):

$$LFM = \begin{pmatrix} 30\% & GSI \le 0.5 \\ 440 * GSI - 190 & GSI > 0.5 \end{pmatrix} \tag{10}$$

The maximum LFM value is 250% when GSI is 1. The daily CI was then computed from the LFM value Eq. (10) based on a blend of relationships included in NOAA (2022b) and (NWCG 2023; C. Schultz, personal communication), and scaled to a range from 0.0 to 1.0:

$$CI_{GSI} = \begin{pmatrix} 100 & LFM = 30\% \\ -0.811 * LFM + 124.3 & 30\% < LFM < 120\% \\ -0.811 * LFM + 120.3 & 120\% \le LFM < 150\% \\ 0 & LFM \ge 150\% \end{pmatrix} \tag{11}$$

When the LFM is 30% the fuels are considered completely cured or dried out and for LFM ≥150% the vegetation is considered completely green. Other than the differences in the meteorological variables observed at the RAWS locations there were no distinctions between the GSI values estimated for the grassland or shrubland land covers associated with the RAWS observations.

The daily CI values estimated for grassland and shrubland RAWS stations with the satellite-based GVF were derived during March through November of 2021 and 2022. The GVF values were estimated from daily NDVI that were interpolated from weekly maximum *GOES* ABI NDVI values. The NDVI values used to compute the weekly maximum NDVI values were based on cloud-screened visible and near-IR data using the ABI daily Clear Sky Mask (www.goes-r.gov/products/baseline-clear-sky-mask.html) product. The CI derived from the GVF values (CI_{GVF}) was compared with the CI estimated from the GSI (CI_{GSI}). The daily GVF values (GVF_i) ranged from 0.0 to 1.0 and the daily CI_{GVF} was estimated as:

$$CI_{GVF} = (1.0 - GVF_i) \tag{12}$$

c. Derivation of the Grassland Fire Danger Index

The GFDI was derived daily from both the atmospheric (CI_{GSI}) and satellite-based (CI_{GVF}) estimates of the CI at the 47 RAWS stations shown in Fig. 1. The formula for GFDI is:

$$GFDI = 10^{(0.009254 - 0.004096(100 - CI)^{1.536} + 0.01201T + 0.2789\sqrt{V} - 0.09577\sqrt{RH}} \tag{13}$$

based on Schreck et al. 2010), where:

CI is the curing index, estimated by the GSI or GVF, expressed as a percentage,
T is air temperature, in °C,
V = sustained wind (km h^{-1}) at 10 m,
RH is relative humidity, expressed as a percentage.

All of the meteorological values within Eq. (13) were observed at 2100 UTC from the RAWS stations. Typically, stations in the Great Plains have their maximum temperature and minimum relative humidity around this time of day (Betts and Tawfik 2016). RAWS stations measured wind at 6.1 m (20 ft) and some stations may use a cup or propeller anemometer rather than a sonic anemometer to measure wind speed. Using 6.1 m and/or a cup or propellor anemometer can result in lower recorded wind speeds than at 10 m (Finkelstein et al. 1986, Lindley et al. 2011, Fovell and Capps 2025). No adjustment was made to the observed 6.1 m wind speeds, because the impact likely varies because of differences in land cover and instrumentation across the region. Because the 6.1 m wind speed was lower than a 10-m wind used to calculate GFDI in Eq. (13), the NDFRS Fire Danger would be underestimated on some days.. The impact would be the same whether using CI_{GVF} or CI_{GSI}, because both included the same meteorological variables and would not impact the results described below.

3. Analysis and discussion

a. Estimation of GVF from Advanced Baseline Imager NDVI

Analysis of the linear regression models indicated that there were two significantly different models ($p < 0.01$) for estimation of the growing season GVF of grasslands and shrublands (Fig. 2). *GOES* ABI NDVI was associated with 87% of the variance in the GVF at the RAWS stations dominated by a land cover of grasslands and 72% of the variance in the GVF at stations dominated by a land cover of shrubland (Table 2). The RMSE associated with the grassland model was 7% (0.07), while 8% (0.08) for the shrubland model. Although monthly models were evaluated for each land cover, the amount of variance in the GVF associated with the NDVI was greater for the seasonal models than the majority of the monthly models.

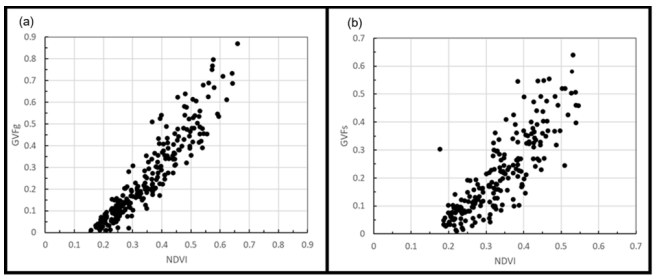

Figure 2. Relationship between Green Vegetation Fraction (GVF) and Normalized Difference Vegetation Index (NDVI) observed at RAWS stations in 2021 and identified as a) grassland b) and shrubland land covers.

b. Evaluation of Curing Index based on GSI and GVF

CI_{GSI} and CI_{GVF} were calculated for each day meteorological data was available at the locations shown in Fig. 1. The March through November distribution of the CI differed between the two estimators (GSI and GVF) for both grassland and shrubland locations (Fig. 3). Generally, the CI_{GSI} displayed a bimodal distribution. For grasslands, the CI_{GSI} distribution had a maximum around 100% (fully cured) and a second near 0% (fully green) during both years. The primary difference from 2021 to 2022 was a larger number of CI_{GSI} values that were <50% in 2021. For the CI_{GVF}, greater than half of the values were between 50 and 90%. Less than a quarter of observations had a curing index <50%. The interquartile range (IQR) within the CI_{GSI} and CI_{GVF} datasets were similar in 2021 and 2022.

The shrublands CI_{GSI} also showed a bimodal distribution (Fig. 3b and 3d). The bimodal distribution was more evident in 2021 than 2022 because an extreme to exceptional drought (droughtmonitor.unl.edu/data/png/20220315/20220315_usdm.png) impacted much of New Mexico and western Texas in the spring of 2022. The shrubland CI_{GVF} had half of its observations between 65% and 90% with few observations <50%. The median

Table 2. Results of statistical analysis of the relationship between NDVI and the Green Vegetation Fraction (based on Eq. 1) for Grassland (GVF_g) and Shrublands (GVF_s) for United States Great Plains RAWS stations.

Variable	b_0	b_1	r^2	RMSE	n
GVF_g	–0.28	1.52	0.87	0.07	231
GVF_s	–0.22	1.30	0.72	0.08	220

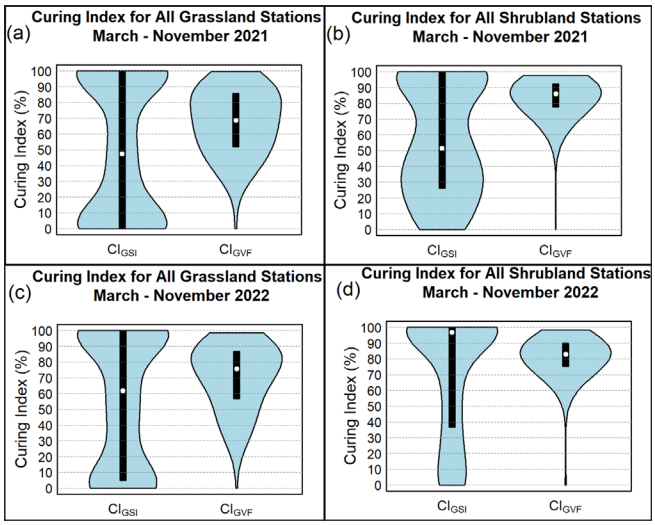

Figure 3. Violin plot of the distribution of daily CI_{GSI} and CI_{GVF} for all stations: a) grassland locations for all days in 1 March–30 November 2021, b) shrubland locations for 1 March–30 November 2021, c) grassland locations for all days for 1 March–30 November 2022 and d) shrubland locations for all days for 1 March–30 November 2022. The white circle represents the median of the distribution and the bottom (top) of the black bar represent the 25th (75th) percentile of the distribution.

CI was higher in 2022 than 2021 regardless of how CI was calculated, although the median was more than 40% greater in 2022 for the CI_{GSI} while only 5% greater for the CI_{GVF}. Similar to grasslands, the CI_{GSI} had a larger IQR than CI_{GVF}.

The distribution of CI was also examined by season for spring (1 March–31 May), summer (1 June–31 August), and autumn (1 September–30 November) for each year (Fig. 4). For grasslands, the CI_{GSI} had relatively few values in spring that were between 30 and 70% (Fig. 4a). Three-quarters of CI_{GVF} values were >60% with no values <20%. As grasses continued to green in summer, the median values of both estimates of CI decreased with the CI_{GSI} calculation having a median value of 20% compared to >50% for CI_{GVF} (Fig. 4c). Despite the lower median, the 75th percentile for the CI_{GSI} and CI_{GVF} was nearly the same and there were more CI_{GSI} values >90%. The IQR for CI_{GVF} was ~20% — less than half of the IQR for CI_{GSI}. CI_{GSI} again showed a bimodal distribution in autumn (Fig. 4e). CI_{GVF} had a median similar to spring in autumn although the tail of the distribution extended to lower values. For 2022 (not shown) the results were similar to 2021, (e.g., during the summer), both CI_{GSI} and CI_{GVF} had a high number of days with CI >50% and the IQR was larger for both estimates.

For shrubland, a higher percentage of CI_{GSI} values were <50% in spring (Fig. 4b) and autumn (Fig. 4f). The median value of CI_{GSI} was the same in spring and summer (Fig. 4d) although the 75th percentile was lower in summer. The CI_{GVF} had a smaller IQR for shrubland compared to the CI_{GSI} for all seasons and the median value was higher — from 90% in spring to 70% in summer. In 2022 (not shown), CI_{GSI} had a median value near 100% in both spring and summer. CI_{GVF} was also higher in spring and summer compared to 2021. In both seasons, the IQR for CI_{GSI} was larger than CI_{GVF}. In autumn 2022, CI_{GSI} again had a bimodal distribution similar to 2021 except a larger number of observations near 0%. There was almost no difference between the two years for CI_{GVF}.

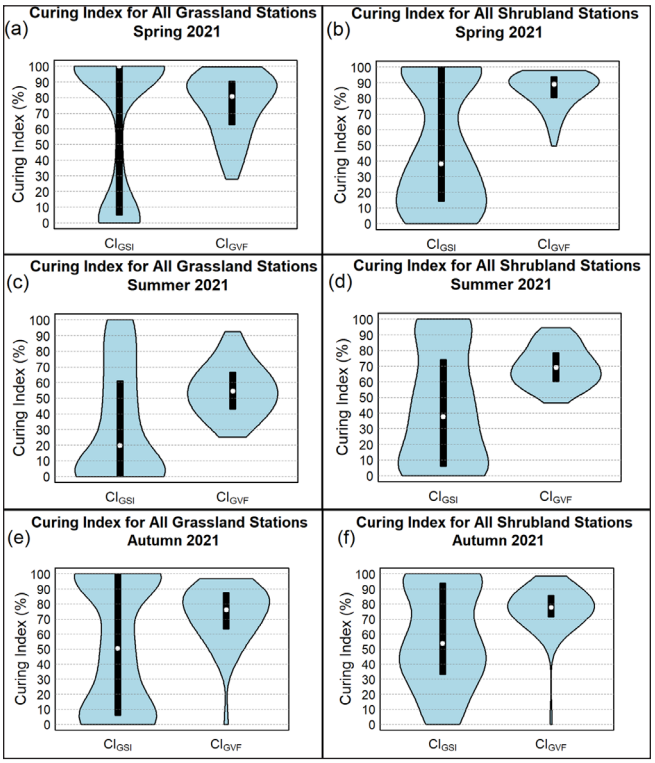

Figure 4. Violin plots of the distribution of daily CI_{GSI} and CI_{GVF} by season and landcover type for all stations. Left column is grassland for a) Spring 2021, c) Summer 2021, and e) Autumn 2021. The right column is shrubland for b) Spring 2021, d) Summer 2021, and f) Autumn 2021.

c. Impact on GFDI of GSI and GVF estimates of Curing Index

The GFDI Eq. (13) was calculated using both CI_{GSI} and CI_{GVF}. The derived GFDI values were converted to categories of fire danger from Schreck et al. (2010), and dashed lines are used within figures to indicate the level of NFDRS grassland fire danger category thresholds (Schreck et al. 2010). The five categories for the grassland fire danger are Low (GFDI values of 0–2), Moderate (3–7), High (8–19), Very High (20–49), and Extreme (≥50). The distribution of GFDI from March through November 2021 (Fig. 5a and b) showed little difference in GFDI categories whether using CI_{GSI} or CI_{GVF}. At least 75% of all days had a Low fire danger for both land cover types. Because fire danger is based on weather components of wind speed, temperature, and relative humidity (Lindley et al. 2011), there were many days where these meteorological variables were not conducive for dangerous fire weather conditions. On those days, differences in CI had little or no impact on the rangeland fire danger category. This was consistent for both years and each season (not shown).

To better determine the impact of different calculations of CI, days with meteorological conditions more conducive to large fires were reviewed. Lindley et al. (2011) examined the weather conditions for large fires in the southern plains from 1 January 2006–10 May 2010. All of the fires in their database occurred when the 6-m wind speed was ≥4.5 m s^{-1} (≥10 mph), temperature ≥4.4ºC (≥40ºF), and the relative humidity ≤35%. These criteria were used to identify days conducive to rapid fire spread. Table 3 shows the percentage of days that had a Moderate or higher fire danger using the restrictive criteria. Half of the restrictive days had at least a Moderate fire danger in grasslands when using CI_{GSI} to calculate GFDI (hereafter $GFDI_{GSI}$) (Fig. 5c) compared to only 42% of days when using CI_{GVF} to calculate GFDI (hereafter $GFDI_{GVF}$). The opposite was observed for shrubland stations in 2021 where almost

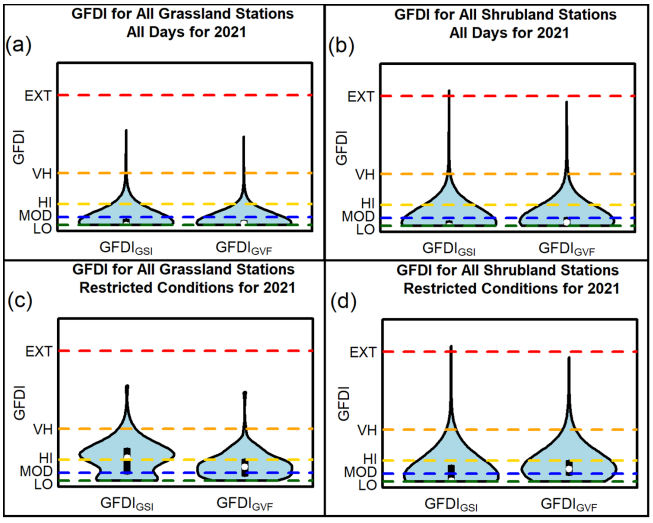

Figure 5. Violin plots of the distribution of daily GFDI using CI_{GSI} and CI_{GVF} for all stations in 2021: a) Distribution of GFDI for all grassland locations, and b) distribution of GFDI for all shrubland locations. Distribution of GFDI for c) all grassland locations and d) all shrubland locations with restricted meteorological conditions based upon Lindley et al. (2011) of relative humidity ≤ 35%, temperature ≥4.4ºC (≥40ºF), and wind speed ≥4.5m s^{-1} (≥10 mph). Dashed lines indicate the minimum value for each fire danger category where "LO" is low, MOD is Moderate, HI is High, VH is Very High, and EXT is Extreme.

Table 3. Percentage of observations with the calculated GFDI in the Moderate Category or higher by year and season for days with restricted meteorological conditions based upon Lindley et al. (2011) of relative humidity ≤35%, temperature ≥4.4ºC (≥40ºF), and wind speed ≥4.5 m s^{-1} (≥10 mph).

Season	Grassland		Shrubland	
	$GFDI_{GSI}$	$GFDI_{GVF}$	$GFDI_{GSI}$	$GFDI_{GVF}$
All Days 2021	50%	42%	36%	70%
Spring 2021	77%	59%	37%	89%
Autumn 2021	46%	50%	38%	60%
All Days 2022	50%	52%	70%	78%
Spring 2022	74%	68%	80%	94%
Autumn 2022	33%	54%	27%	47%

twice as many days had a Moderate or higher fire danger using $GFDI_{GVF}$ compared to $GFDI_{GSI}$ (Fig. 5d). In 2022, the two calculations produced a similar percentage of days with a Moderate or higher fire danger in grassland locations with $GFDI_{GVF}$ resulting in more days with a Moderate or higher fire danger in shrubland locations.

The fire danger categories were examined by season, with only spring and autumn shown as larger fires tend to occur during the transition seasons (Lindley et al. 2011). For grasslands in spring, $GFDI_{GSI}$ had more days with Moderate or higher fire danger than $GFDI_{GVF}$ in both 2021 and 2022 (Fig. 6a and 6e and Table 3). CI_{GSI} was also generally higher than CI_{GVF} in spring in grasslands (Fig. 4). With higher CI_{GSI} values compared to CI_{GVF} in grasslands, the same meteorological conditions will result in a higher GFDI. In autumn, when CI_{GVF} was greater than CI_{GSI} (Fig. 4), the $GFDI_{GVF}$ displayed a greater number of days with a Moderate or higher fire danger (Fig. 6c and 6g). The difference was larger in 2022 as only one-third of days had at least a Moderate fire danger using $GFDI_{GSI}$ compared to over half of days using $GFDI_{GVF}$. For shrubland locations in spring 2021, most days had a Moderate or higher fire danger when using $GFDI_{GVF}$ (Fig. 6b and 6f) while less than half of days reached Moderate using $GFDI_{GSI}$. In 2022, both calculations of GFDI resulted in >75% of the days with a Moderate or greater fire danger. In autumn, 20% more days had at least a Moderate Fire Danger when using $GFDI_{GVF}$.

The daily mean CI_{GSI} and CI_{GVF} were calculated for both years for grasslands and shrublands (Fig. 7). Similar to the violin plots (Fig. 3 and 4), the CI_{GSI} had a larger range and more variance during the year than CI_{GVF}. Multiple minima and maxima were seen throughout the year where CI_{GSI} changed by more than 30% in less than a couple of weeks. For the grasslands, there were at least two minima observed in both years — one was in late spring and early summer and another was in early to mid-autumn. In 2021, there was another minimum in July. For shrublands, both years showed several minimum values in autumn. In 2021, there were minima in spring and mid-summer. As noted earlier, there was an extreme to exceptional drought across most of New Mexico and portions of western Texas by late May 2022 and CI_{GSI} was >70% in spring and summer. For both grasslands and shrublands, and in both years, the CI_{GSI} displayed a decrease in CI (green-up of vegetation) around 1 October.

The CI_{GVF} only showed a single minimum for both land covers in both years. For grasslands, this minimum was in the early summer and for shrublands the minimum was in late summer or early autumn. For both land covers, the CI_{GVF} was increasing in autumn at a time when CI_{GSI} had a minimum. With winter approaching, this period in vegetation development normally corresponds to a time of vegetation senescence (aging and deterioration within vegetation), rather than green-up (as implied by the low CI_{GSI} values).

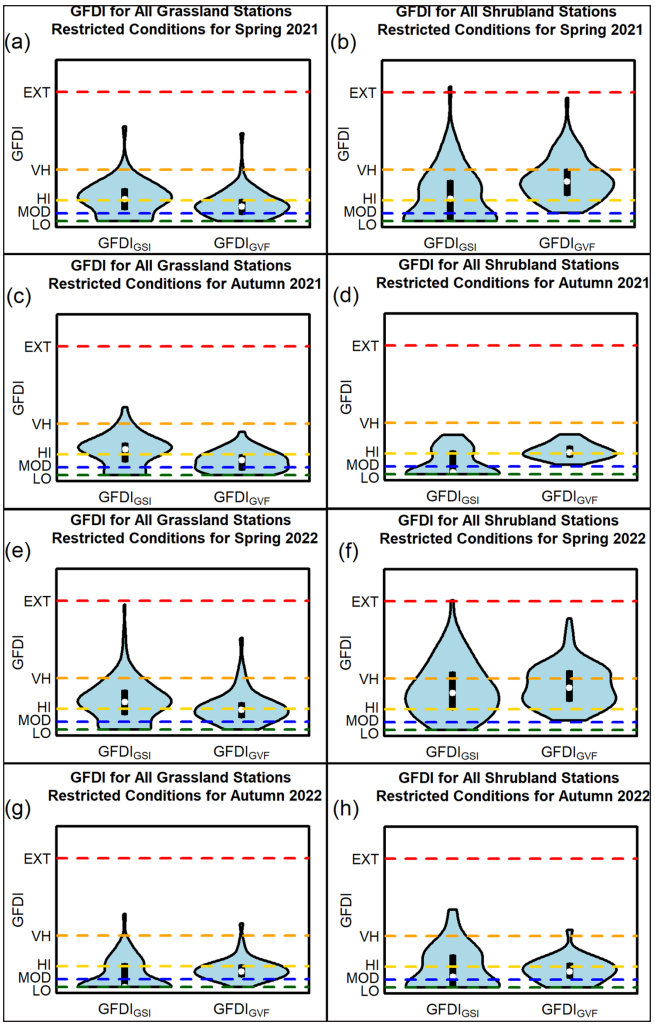

Figure 6. Distribution of $GFDI_{GSI}$ and $GFDI_{GVF}$ during spring and autumn days for all stations on restricted meteorological conditions of relative humidity ≤35%, temperature ≥4.4ºC (≥40ºF), and wind speed ≥4.5 m s^{-1} (≥10 mph). Left column is for grassland in a) Spring 2021, c) Autumn 2021, e) Spring 2022 and g) Autumn 2022. The right column is for shrubland in b) Spring 2021, d) Autumn 2021, f) Spring 2022, and h) Autumn 2022.

A comparison of GFDI for 5 grassland stations and 5 shrubland stations shows the impact differences in the estimation of CI had on the computed fire danger (Fig. 8). The October minima in CI_{GSI} seen in Fig. 7a through 7d corresponds to when the $GFDI_{GSI}$ is lower than the $GFDI_{GVF}$ (Fig. 8). At all 10 stations, the $GFDI_{GVF}$ had several days of Moderate to High fire danger while $GFDI_{GSI}$ was Low. In the summer of 2022 when the CI_{GSI} was >70% in July and August, the $GFDI_{GSI}$ had several days of Moderate to High fire danger at all grassland stations (Fig. 8a). With CI_{GVF} lower, $GFDI_{GVF}$ was a Low fire danger for most days in July and August.

A closer examination of both CI and GFDI values from a grassland site 3.3 km west of Gering, Nebraska, (SBFN1) and a shrubland site 16.4 km south of Barnhardt, Texas, (BNHT2) from 2022 illustrated the differences in GFDI due to the use of either CI_{GSI} and CI_{GVF} (Fig. 9). Similar to the mean time series for all grassland locations (Fig. 7c), the CI_{GVF} at SBFN1 showed a relatively smooth change from spring through autumn (Fig. 9a). The grassland vegetation began to green in May and had a minimum curing index in July and August. As vegetation senesced during autumn months in western Nebraska, the CI_{GVF} increased to >90% by November. The CI_{GSI} had greater variability. The CI_{GSI} was at 100% through April before decreasing to <20% in May. Values remained <50% for approximately 30 days. The CI_{GSI} then increased to 100% in mid-summer at the same time the CI_{GVF} was at its minimum. The CI_{GSI} remained >50% until late September when it decreased to 0% for a 20-day period in October when CI_{GVF} increased. In less than 10 days, the CI_{GSI} then increased to 100% by late October. Due to the high CI_{GSI} values from mid-July to mid-August, the $GFDI_{GSI}$ was consistently at or above the Moderate level (Fig. 9c) while $GFDI_{GVF}$ was consistently in the Low category.

At the shrubland station BNHT2 (Fig. 9b), there were several minimum values in CI_{GSI} while CI_{GVF} only had one minimum. The first significant minimum was around May 1 when the CI_{GSI} fell below 50% for several days. The CI_{GVF} showed little change during this period with values near 90%. An autumn minimum was also

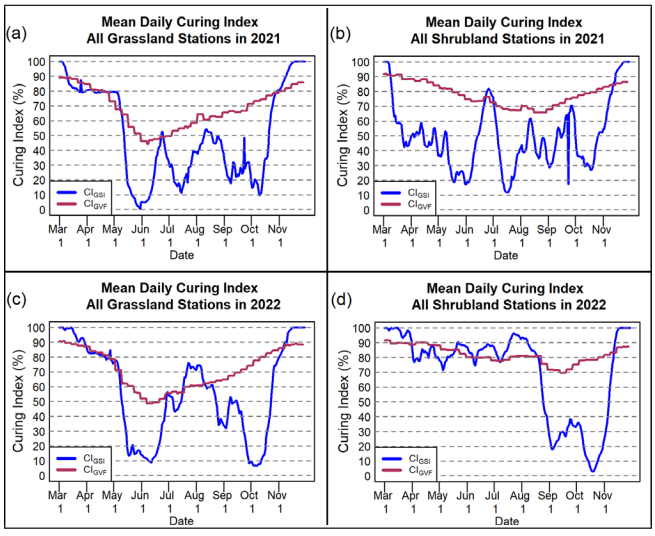

Figure 7. The daily mean Curing Index from 1 March–30 November for all grasslands (left) in a) 2021 and c) 2022. and for all shrublands (right) in b) 2021 and d) 2022. The blue line is CI_{GSI} and the red line is the CI_{GVF}.

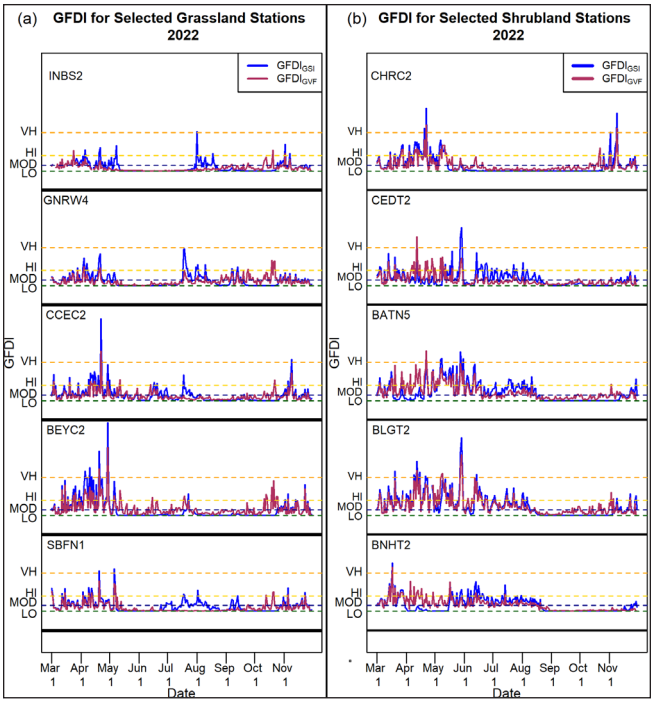

Figure 8. Time series of $GFDI_{GSI}$ and $GFDI_{GVF}$ fire danger categories from 1 March–30 November 2022 for a) grassland stations INBS2 (54 km north of Belle Fouche, South Dakota), GNRW4 (9.8 km northwest of Hartville, Wyoming), CCEC2 (1.6 km south of Plainview, Colorado), BEYC2 (4.9 km east-southeast of Buckeye, Colorado), and SBFN1 (3.3 km west of Gering, Nebraska), and b) shrubland stations CHRC2 (3.3 km south-southwest of Deckers, Colorado), CEDT2 (11.5 km southwest of Fritch, Texas), BATN5 (34.4 km southwest of Carlsbad, New Mexico), BLGT2 (Bootleg, Texas), and BNHT2 (16.4 km south of Barnhardt, Texas).

observed for both estimates of CI. As with SBFN1, the CI_{GSI} decreased to 0% for much of autumn while the CI_{GVF} dropped to <70% in late September. The decrease in CI_{GSI} was more rapid going from 100% to 0% in less than 10 days. CI_{GVF} reaches its minimum value after 30 days. The greatest difference in GFDI occurred in spring. Because of lower CI_{GSI}, $GFDI_{GSI}$ rarely had a Moderate or higher fire danger from early April through mid-May. However, because CI_{GVF} remained near 90%, the $GFDI_{GVF}$ consistently calculated a Moderate (Fig. 9d) fire danger with several days having a High fire danger.

Because differences in the GFDI values were only due to the differences in the CI, the CI_{GSI} was examined further. The GSI is based upon 3 components — minimum temperature, photo period, and VPD. Figures 10 and 11 show each component of GSI, the computed GSI, and the resultant CI_{GSI} for SBFN1 (Fig. 10) and BNHT2 (Fig. 11), respectively.

At SBFN1, the day length was <11 h from early March through mid-October and iPhoto was set to 1 for that period (Table 1, Fig. 10a). Similarly, iT_{min} was set to 1 when the minimum temperatures were 5ºC (41ºF) or greater. Because temperatures <5ºC occurred into late spring, iT_{min} was <1 into early May and then remained at 1 from late May through early October (Fig. 10b). The

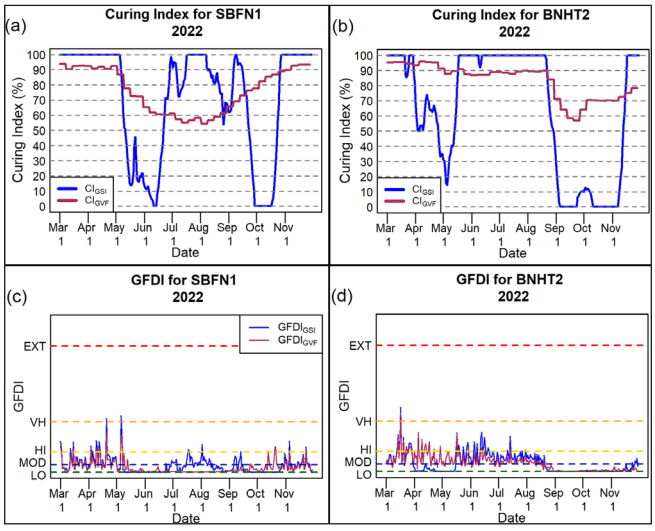

Figure 9. Top row: Time series of CI_{GVF} (red line) and CI_{GSI} (blue line) from 1 March–30 November 2022 at a) 3.3 km west of Gering, Nebraska, (SBFN1, Grassland location) and b) 16.4 km south of Barnhardt, Texas (BNHT2, Shrubland location). Bottom row: Time series of GFDI using CI_{GVF} (red line) and CI_{GSI} (blue line) at c) SBFN1 and d) BNHT2.

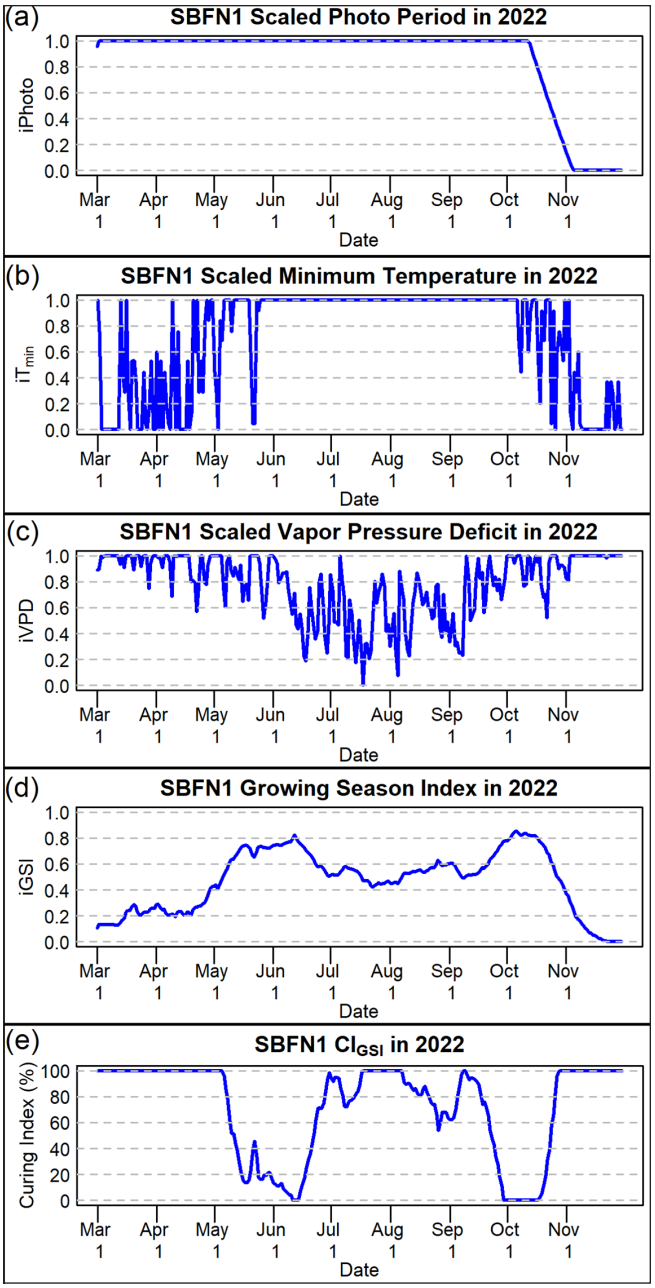

Figure 10. Time series of a) scaled photo period, b) scaled minimum temperatures, c) scaled vapor pressure difference, d) the 21-day mean GSI, and e) the CI_{GSI} estimated from the 21-day mean GSI from 1 March–30 November 2022 for 3.3 km west of Gering, Nebraska (SBFN1).

iVPD (as per Table 1, inverse relationship with actual VPD) varied throughout the warm season (Fig. 10c). An annual cycle was evident in VPD and iVPD. There are minima of VPD (maxima iVPD) in late spring and mid-autumn and a maximum in VPD (minimum iVPD) from July into early September (Fig. 10c). Within this broader cycle, daily values of iVPD changed by more than 0.5 within a week. The 21-day mean GSI (Fig. 10d) had a similar annual cycle as the scaled VPD (Fig. 10c). The resulting CI_{GSI} values (Fig. 10e) generally displayed an inverse relationship to the GSI values.

The photoperiod at BNHT2 was similar to SBFN1, with iPhoto set to 1 March 1 through late October (Fig. 11a). The minimum temperature was >5ºC (41ºF) from April 1 through November and iT_{min} remained at 1 during this period (Fig. 11b). The iVPD had a similar annual cycle to SBFN1 except extending over a longer period of time (Fig. 11c). VPD had minima (iVPD maxima) in early spring and late autumn and a maximum (iVPD minimum) in mid-summer. Within this broader annual cycle, the daily iVPD again varied by >0.5 over a week throughout the summer. The 21-day mean GSI followed a similar annual cycle as the iVPD from late April into early October (Fig. 11d).

There were maxima in GSI and VPD for both stations (and land covers) in May and September into October with a minimum during the summer. When VPD was near a minimum (iVPD maximum) in late spring and autumn (Fig. 10c and 11c), GSI was near a maximum (Fig. 10d and 11d) and the corresponding CI_{GSI} was at a minimum (indicating a greater percentage of green vegetation — Fig 10e and 11e).

The variability in GSI in the warm season can primarily be attributed to the variability in VPD. When temperatures were relatively cooler in late spring and mid-autumn, there was enough moisture near the surface to decrease the actual VPD. The mean CI_{GSI} shown in Fig. 7 also had a minimum in late spring and early to mid-autumn. Decreasing VPD resulted in CI_{GSI} near zero in late spring and early to mid-autumn across the Great Plains. In summer, when VPD was near a maximum, GSI was also near a minimum and CI_{GSI} reached a maximum (indicating brown vegetation). Although the mean time series shown in Fig. 7a and 7c did not show CI_{GSI} increasing to 100%, most stations saw VPD increase during this time, which resulted in a summer maximum in CI_{GSI}.

For grasslands, the minimum CI_{GVF} was in early to mid-summer when GVF (and NDVI) was near its maximum (Fig. 7a and 7c). The CI_{GSI} summer minimum

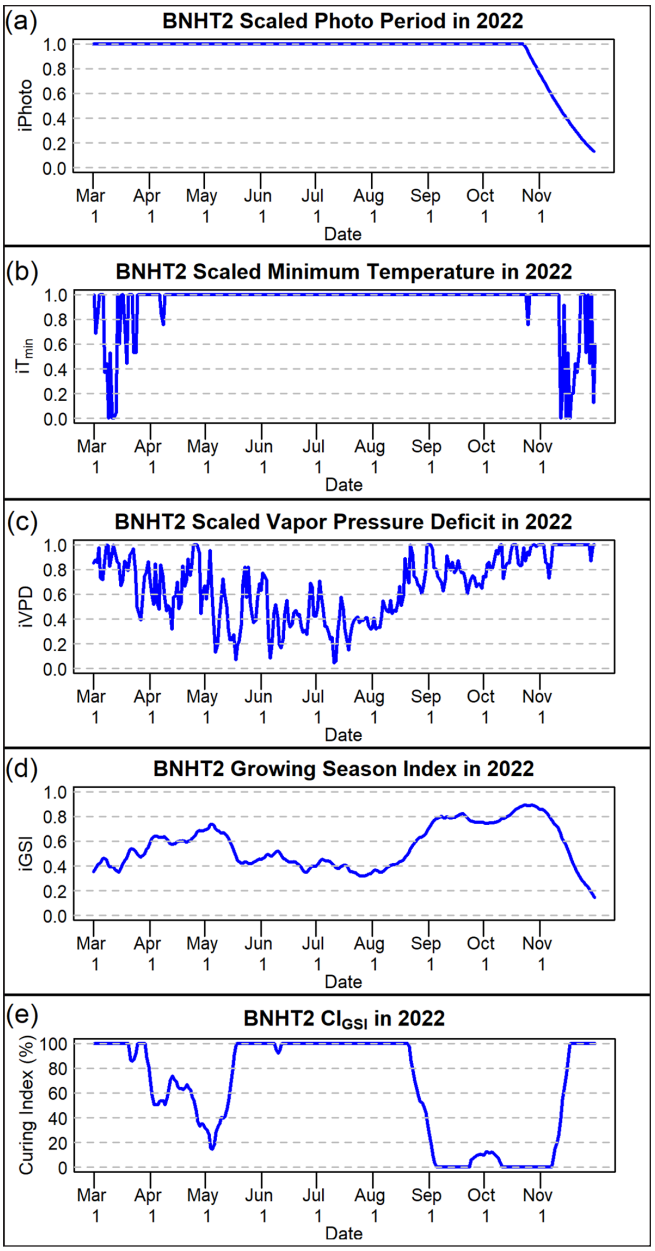

Figure 11. As in Fig. 10, except for 16.4 km south of Barnhardt, Texas.

caused by increasing VPD was not observed in CI_{GVF}. In autumn, CI_{GVF} increased as GVF decreased with vegetation browning at the end of the growing season. The minimum in CI_{GSI}, due to the decreased VPD in autumn, was not observed in the CI_{GVF} time series. For shrublands, the largest differences were in spring and autumn. CI_{GVF} showed a slow decrease through spring in both the mean time series (Fig. 7b and 7d) and at BRNT2 (Fig. 9b) indicating only small changes in GVF. Both in the mean time series in 2021 and at BRNT2, CI_{GSI} showed a rapid decrease and remained low through spring. This minimum corresponded to a time when the actual VPD was near a minimum in late spring. In autumn, while both CI_{GSI} and CI_{GVF} reached a minimum, the minimum CI_{GSI} in late October occurred at a time CI_{GVF} was increasing. As with grasslands, this minimum in CI_{GSI} corresponded to a time when the scaled VPD was near 1 implying actual VPD was low.

The impact of these differences was reflected in the NDRFS fire danger category computed using GFDI (Fig. 9c and 9d). Generally, when actual VPD was near a minimum and CI_{GSI} was lower than CI_{GVF} (late May-early June and early to mid-October, Fig. 9a), the $GFDI_{GVF}$ and fire danger was higher (Fig 9c). Many other grassland and shrubland sites had a similar difference in GFDI during October (Fig. 8). When actual VPD was near a maximum and CI_{GSI} was higher than CI_{GVF}, as occurred in summer, there were more days with a Moderate or higher fire danger when using CI_{GSI} (Fig. 8a). This is because with higher afternoon temperatures, even with wind speeds <4.5 m s^{-1} (10 mph), a Moderate or higher rangeland fire danger can occur if the CI is >90%. During this same period, the GFDI using CI_{GVF} had a Low fire danger as it would require winds >8.9 m s^{-1} (20 mph) to get above a Low fire danger when CI < 60%.

The observed differences in GFDI based on the use of CI_{GVF} and CI_{GSI} might be attributed to the initial development of GSI as a parameter to generalize the greenness and health of vegetation in different climates with different plant species across the world (Jolly et al. 2005). The GSI was determined to be useful for reconstruction of historical variation in phenological responses as well as forecasting future responses due to changing climatic conditions. GSI is also sensitive to unfavorable (favorable) atmospheric conditions for growth that can result in rapid browning (greening) of vegetation and may predict that CI is undergoing rapid changes before it is apparent from satellite observations. Daham et al. (2019) noted that using VPD alone to assess the impact of moisture on vegetative greenness resulted in a poor prediction for vegetative greenness in semi-arid areas of Iraq. They included a precipitation term to the GSI to improve the performance of the model in semi-arid regions. The GSI results, with and without the precipitation term, were compared to NDVI values derived on a 16-day interval from the National Aeronautics and Space Administration (NASA) Moderate Resolution Imaging Spectroradiometer (MODIS) sensor. For all four study sites examined the correlations between GSI and NDVI values were improved when the GSI model included the precipitation term. Based on the Daham et al. (2019) results, Jolly et al. (2024) included a precipitation term in the GSI used within the live fuel moisture model within the US National Fire Danger Rating System (USNFDRS; Jolly et al., 2024) and they also evaluated fine-tuning GSI for 6 different fuels across the United States.

An evaluation of GSI, including a precipitation term (Jolly et al. 2024), is currently in progress within the National Weather Service (C. Schultz, personal communication). As the Energy Release Component (ERC, Cohen and Deeming 1985; Lindley et al. 2014) is also used for determining fire fuel status at some National Weather Service offices, a cursory comparison of ERC values downloaded from Climate Engine (Huntington et al. 2017) and CI derived from the GSI and GVF was included in this study for site SBFN1 (Fig. 12). The trends between the ERC values and the CI_{GVF} appear similar during the June through mid-October timeframe with both variables generally increasing. However, in March and April, the ERC is increasing while CI is decreasing,

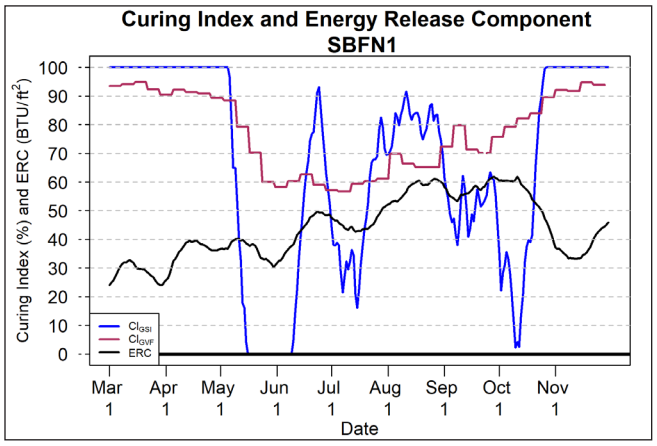

Figure 12. The CI_{GSI} (blue line), CI_{GVF} (red line), and 21-day average ERC (black line) from 1 March–30 November 2021 at SBFN1. ERC data from Climate Engine are in BTU ft^2 where 1 BTU ft^{-2} = 11356.5 J m^{-2}.

which would result in differing interpretations of how susceptible fuels are to fire growth. A more extensive comparison of the ERC and CI estimates is recommended.

Estimation of GVF from NDVI derived from *GOES* ABI observations provided a viable method to estimate CI. NDVI measures changes in greenness once it is visible in vegetation due to meteorological conditions that occur over multiple days or weeks. Limitations to the use of a weekly GVF value derived from a maximum NDVI value, as within this study, includes the possibility of underestimation (overestimation) of the GVF during times of rapidly changing vegetative greenness such as may occur in springtime (autumn). Figure 7 shows that changes in CI_{GVF}, as used within this study, are more gradual than CI_{GSI}. However, because the *GOES* ABI provides 5-min observations across the Great Plains, it may be possible to create the same product for a smaller time window by using images from multiple times of day such that rapid changes in greenness may be observed. Future development of a daily (or hourly) *GOES* ABI GVF product should provide a more robust estimate of GVF than reliance on the relationship between NDVI and GVF developed within this study.

4. Conclusion

Determining fire fuel status remains a challenge across the Great Plains. Where crops do not exist, grasses and shrubs are the primary land cover. A survey of NWS offices across the Great Plains indicated no consistent methodology for determining the moisture level in vegetation (CI) with some offices relying on subjective observations. The different methods for estimating CI can result in different forecast fire danger. The difference in forecasts of fire danger can impact decisions by fire partners to do prescribed burns, prepare for dangerous fires, and NWS forecasters to issue Red Flag Warnings. Because dry fuels are critical to rapid fire spread, an objective measure for estimating CI across the entire Great Plains is needed that improves both the issuance of Red Flag Warnings and the consistency of information provided to fire responders on the danger of rapid-fire growth due to both dry fuels and favorable meteorological conditions. Improved briefings and warnings could help fire responders better prepare for extreme fire behavior so they can limit the risk to life and property.

This study compared two methods of estimating the CI, an indicator of the moisture level of vegetation included in the Grassland Fire Danger Index; i) a satellite method using data from *GOES* ABI and ii) a method using the GSI that uses meteorological conditions to estimate plant growth. The satellite-based estimate of the CI (CI_{GVF}) included a model developed relating *GOES* ABI observed NDVI to the CI based upon the VIIRS GVF. The meteorological observation-based GSI was used to estimate the Live Fuel Moisture to find the CI (CI_{GSI}). Both estimates were applied to RAWS locations in the Great Plains where either grasses or shrubs were the primary land cover.

These results showed there can be large differences in the CI depending on whether satellite data (CI_{GVF}) or meteorological data (CI_{GSI}) was used in its estimation. CI_{GVF} showed a gradual change through the year with a minimum in summer to early fall depending whether grasses or shrubs were the primary land cover. CI_{GSI} had larger variability with minima in spring and autumn and a maximum in summer. This pattern was primarily related to the annual change in VPD from spring through autumn. During times of higher (lower) VPD, the CI_{GSI} was higher (lower). The difference in CI between the two methods resulted in differences in the computed fire danger category when using GFDI. For several shrubland stations, the fire danger category using CI_{GVF} was generally higher during October when meteorological conditions were also favorable for fire growth. For several grassland stations, the fire danger category was higher when using CI_{GSI} except in autumn 2022. However, because CI_{GSI} has a larger variability throughout the year, there were times through the warm season when the fire danger differed using CI_{GSI} regardless of land cover type depending on both changes in VPD and when meteorological conditions were favorable for fire growth. For both grasslands and shrublands, and in both years, the CI_{GSI} displayed an autumn green-up that was not observed during the wildfire seasons of 2021 and 2022.

The results suggest that additional evaluation (e.g., intensive field studies) of the CI and its relationship with satellite and meteorological variables are required. Other methods for estimating the susceptibility of fuels to fire growth, such as ERC, which is also used by NWS offices, could be included in future evaluations as ERC can differ from both CI_{GSI} and CI_{GVF} and impact the issuance of Red Flag Warnings. In addition, recommendations include the evaluation of the performance of CI_{GSI} and CI_{GVF}, and resulting GFDI values, on critical fire days. The evaluation of a combined satellite and meteorological estimate of the Curing Index should also be considered. The development of a daily (or hourly) GVF product as part of a future *GOES* suite of land products is also recommended.

Acknowledgments: Much of this research was completed when the first author (Schumacher) worked for the National Weather Service in Sioux Falls, South Dakota and the fourth author (Gallo) was employed with NOAA.

We would like to thank Chauncy Schultz, Dr. Matthew Bunkers (retired), and Em Wong from the National Weather Service for discussions on use of GSI to determine the Curing Index. We would like to thank Chauncy for sharing his algorithm on relating GSI to Curing Index. We also thank Mark DeBruin for his assistance in developing code to upscale the 30-m Crop Data Layer to 500 and 1000 m. This research utilized weather observations for 47 stations from NIFC's RAWS network and were obtained using the Synoptic Data PBC Weather API. Emma Centeno and Britney Wu were supported by the NOAA Hollings Scholarship program in 2022 and 2023, respectively. We would like to thank the management and staff of the National Weather Service in Sioux Falls for hosting Britney during the summer of 2023. We would also like to thank Daniel Nietfeld and Ken Fenton from Global System Laboratory for their support of this research and preparation of this manuscript and Dr. Benjamin Hatchett for his review of this manuscript prior to submission. We also thank Todd Lindley and 2 anonymous reviewers for their recommendations on this manuscript.

The statements, findings, conclusions, and recommendations are those of the authors and do not necessarily reflect the views of NOAA or the U.S. Department of Commerce. This research was supported in part by the NOAA cooperative agreement NA24OARX432C0007, for the Cooperative Institute for Research in the Atmosphere (CIRA).

REFERENCES

Allen, R. G., L. S. Pereira, D. Raes, and M. Smith, 1998: Crop Evapotranspiration, - Guidelines for computing crop water requirements - FAO Irrigation and Drainage Paper No. 56, [Available online at www.fao.org/4/X0490E/X0490E00.htm.]

Betts, A. K. and A. B. Tawfik, 2016: Annual Climatology of the Diurnal Cycle on the Canadian Prairies. *Frontiers in Earth Sci*., 4, 1–23. CrossRef.

Boryan, C., Z. Yang, R. Mueller and M. Craig, 2011: Monitoring US agriculture: the US Department of Agriculture, National Agricultural Statistics Service, Cropland Data Layer Program, *Geocarto International*, **26** (5), 341–358. CrossRef.

Brock, T. D., 1981: Calculating solar radiation for ecological studies. *Ecol. Model*., **14**, 1–19. CrossRef.

Burgan, R. E. and R. A. Hartford, 1993. Monitoring vegetation greenness with satellite data. USDA Forest Service Intermountain Research Station, General Technical Report INT–297, 14 pp. CrossRef.

____, ____, and J.C. Eidenshink, 1996. Using NDVI to assess departure from average greenness and its relation to fire business. USDA Forest Service Intermountain Research Station, General Technical Report INT-GTR-333, 10 pp. CrossRef.

Cohen J. D. and J. E. Deeming, 1985. The national fire-danger rating system: basic equations. General Technical Report PSW-82. Berkeley, CA, USDA Forest Service, Pacific Southwest Forest and Range Experiment Stations, 17 pp. CrossRef.

Daham, A., Han, D., Jolly, W. M., Rico-Ramirez, M., and Marsh, A. (2019). Predicting vegetation phenology in response to climate change using bioclimatic indices in Iraq. *Journal of Water & Climate Change*, **10** (4), 835–851. CrossRef.

Finkelstein, P. L., J. C. Kaimal, J. E. Gaynor, M. E. Graves, and T. J. Lockhart, 1986: Comparison of wind monitoring systems. part I: in situ sensors, *J. Atmos. Ocean. Technol.*, **3**, 583–593. CrossRef.

Forsythe, W., E. J. Rykiel Jr., R. S. Stahl, H. Wu, and Ro. M. Schoolfield, 1995: A model comparison for daylength as a function of latitude and day of year., *Ecol. Model*., **80**, 87–95. CrossRef.

Fovell, R. G. and S. B. Capps, 2025: Sustained wind forecasts from the High-Resolution Rapid Refresh Model: skill assessment and bias mitigation. *Atmosphere*, **16** (16), 1–27. CrossRef.

Huntington, J. L., K. C. Hegewisch, B. Daudert, C. G. Morton, J. T. Abatzoglou, D. L. McEvoy, and T. Erickson, 2017: Climate Engine: cloud computing of climate and remote sensing data for advanced natural resource monitoring and process understanding. *Bull. Amer. Meteor. Soc*., **98**, 2397–2410. CrossRef.

Jolly W. M., R. Nemani, and S.W. Running, 2005: A generalized, bioclimatic index to predict foliage phenology in response to climate. *Global Change Biology*, **11**, 619–632. CrossRef.

____, P. H. Freeborn, L. S. Bradshaw, J. Wallace, and S. Brittain, 2024: Modernizing the US National Fire Danger Rating System (version 4): simplified fuel models and improved live and dead fuel moisture calculations. Environ. Model. Softw. **181**: 106181, 1–18. CrossRef.

JPSS, 2019: Joint Polar Satellite System level 1 requirement document supplement (L1RDS) – final, 120 pp. [Available online at www.nesdis.noaa.gov/s3/2022-03/L1RDS.pdf.]

Lindley, T. T., J. D. Vitale, W. S. Burgett, and M.-J. Beierle, 2011: Proximity meteorological observations for wind-driven grassland wildfire starts on the southern High Plains. *Electron. J. Severe Storms, Meteor.*, **6** (1), 1–27. CrossRef.

____, and Coauthors, 2014: Southern Great Plains wildfire outbreaks. *Electron. J. Severe Storms, Meteor.*, **9** (2), 1–43. CrossRef.

NESDIS, 2021: Green Vegetation Fraction (GVF) NOAA-unique product algorithm theoretical basis document version 4.0, 61 pp. [Available online at https://www.star.nesdis.noaa.gov/jpss/documents/ATBD/ATBD_NVPS_GVF_v4.0.pdf.]

NOAA, 2021a: Storm Events Database. [Available online at www.ncei.noaa.gov/stormevents/eventdetails.jsp?id=992210.]

____, 2021b: Storm Events Database. [Available online at www.ncei.noaa.gov/stormevents/listevents.jsp?eventType=%28Z%29+Wildfire&beginDate_mm=12&beginDate_dd=15&beginDate_yyyy=2021&endDate_mm=12&endDate_dd=31&endDate_yyyy=2021&county=ALL&hailfilter=0.00&tornfilter=0&windfilter=000&sort=DT&submitbutton=Search&statefips=20%2CKANSAS.]

_____, 2022a: Storm Events Database. [Available online at www.ncei.noaa.gov/stormevents/eventdetails.jsp?id=1023013.]

_____, 2022b: Grassland Curing Guide. [Available online at www.weather.gov/media/dmx/FireWx/CuringGuide2022.pdf.]

____, 2023: [Available online at www.aev.class.noaa.gov/saa/products/welcome;jsessionid=58008731E1EC6B1B6FAE32C960D017BC.]

____, 2024: Weather related fatality and injury statistics [Available online at https://www.weather.gov/hazstat]

Nobel, I. R., A. M. Gill, and G. A.V. Bary, 1980: McArthur's fire danger meters expressed as equations. *Australian J. of Ecology* **5**: 201–203. CrossRef.

NWCG, 2023: National Wildfire Coordinating Group (NWCG) Guide to Fire Behavior Assessment, PMS 437-1, 118 pp. [Available online at www.nwcg.gov/publications/pms437-1.]

Schmit, T. J, P. Griffith, M. M. Gunshor, J. M. Daniels, S. J. Goodman, and W. J. Lebair, 2017: A closer look at the ABI on the GOES-R Series. *Bull. Amer. Meteor. Soc.*, **98**, 681–698, CrossRef.

Schreck, M-B., P. J. Howerton, and K. R. Cook, 2010: Adapting Australia's Grassland Fire Danger Index for the United States' Central Plains. National Weather Service Central Region Technical Attachment Number 10–02. [Available online at www.weather.gov/media/crh/publications/TA/TA_1002.pdf].